Electronic Supplementary Material (ESI) for Journal of Materials Chemistry A.

Supporting Information (SI)

A Rare Case of Iodinated Non-Fullerene Acceptors for High-Performance Organic Solar Cells without Post-Treatments

Hongbin Chen†,[a], Xiangjian Cao†,[a], Peiran Wang[a], Fangfang Huang[a], Yunxin Zhang[b], Huazhe Liang[a], Xingqi Bi[a], Tengfei He[b], Wanying, Feng[a], Yaxiao Guo,[c] Zaifei Ma[d], Guankui Long[b], Zhaoyang Yao*,[a], Bin Kan[b], Chenxi Li[a], Xiangjian Wan[a], Yongsheng Chen*,[a]

[a]State Key Laboratory and Institute of Elemento-Organic Chemistry, The Centre of Nanoscale Science and Technology and Key Laboratory of Functional Polymer Materials, Renewable Energy Conversion and Storage Center (RECAST), College of Chemistry, Nankai University, Tianjin 300071, China.

[b]School of Materials Science and Engineering, National Institute for Advanced Materials, Renewable Energy Conversion and Storage Center (RECAST), Nankai University, 300350, Tianjin, China.

[c]State Key Laboratory of Separation Membranes and Membrane Processes, School of Chemistry, Tiangong University, Tianjin 300387, China.

[d]State Key Laboratory for Modification of Chemical Fibers and Polymer Materials, Center for Advanced Low-dimension Materials, College of Materials Science and Engineering, Donghua University, Shanghai 201620, China.

†These authors contributed equally: Hongbin Chen, Xiangjian Cao.
Corresponding E-mails: yschen99@nankai.edu.cn (Y.C.); zyao@nankai.edu.cn (Z.Y.).

Contents

1. Materials and Methods

2. Synthesis of CH45

3. Figures and Tables

4. References

1. Materials and Methods.

Materials.

Polymeric donor PM6 was purchased from Organtec.Ltd. The end unit INCN-2F was purchased from Woerjiming (Beijing) Technology Development Institute, respectively. starting material 1-1 was synthesized according to our previously reported method.[1] All the other reagents and chemicals were purchased from commercial suppliers and were used directly without further purification unless otherwise noted. The overall synthesis route and detailed synthesized procedures of CH45 and the corresponding characterizations were displayed in “Synthesis of CH45” below.

Methods.

Computational method. The ground-state (S0) geometries of studied molecules, energy level of frontier molecular orbital and the reorganization energy were optimized by density functional theory (DFT) using the Becke three-parameter Lee-Yang-Parr (B3LYP) hybrid functional.[2] The 6-31G(d)[3] and the quasi-relativistic pseudopotentials LANL2DZ[4] basis sets were employed for light C, H, O, N, S F Cl atoms and heavy Br, I atom, respectively. All the alkyl chains were replaced with methyl groups (-CH3) to reduce the computational requirements. And the vibrational frequencies were calculated after geometries optimization and no imaginary frequency was found. All the calculations were performed in the Gaussian 16 package. Besides,[5] the Mercury software was employed to obtain the π-π stacking interaction energy.

Relative dielectric constant (ε_r) test.[6] The capacitance-frequency of CH4 and CH45 neat and blend films were performed in the range of 100Hz to 1MHz using Zennium-E under dark conditions and analyzed with the Zahner Analysis software. Between 10K Hz and 1M Hz, a flat capacitive response with respect to frequency is obtained. Relative dielectric constant (ε_r) can be calculated according to:

$$\varepsilon_r = \frac{C_p \times D}{A \times \varepsilon_0}$$

Where Cp is the measured capacitance; D is the thickness of film; A is the contact area and ε_0 is the permittivity of free space.

Temperature-dependent Photoluminescence (PL) spectra.[7] The temperature-dependent PL spectra varied from 130 to 300 K were conducted by using FLS1000 equipment. The E_b values were obtained by fitting the temperature-varying PL intensities, $I(T)$, with the Arrhenius equation: $I(T) = I_0/(1+A\bullet e^{-(E_b/k_BT)})$. Where I_0 is the PL intensity at the lowest temperature; T is the temperature; A is a constant; k_B is the Boltzmann constant.

Exciton Binding Energy Calculations.[7-8] Exciton binding energy is defined as the difference between the fundamental transport gap (E_g^t) and the optical gap (E_g^O), $E_b = E_g^t - E_g^O$. E_g^t is calculated as the energy difference between the ionization potential (IP) and electron affinity (EA), $E_g^t = IP - EA$, with $IP = E_+ - E_0$ and $EA = E_0 - E_-$, where E_0, E_+, and E_- denote the total potential energies of the ground state (S_0) and the cationic and anionic states, respectively. E_g^O is the excitation energy of the first singlet excited state (S1). In the gas phase, the calculations were performed on the isolated molecules extracted directly from the optimized crystal structure. The S0 and ionic states were calculated by DFT while the S1 state was calculated by time-dependent DFT (TDDFT) with the long-range corrected (LRC) functional ωB97XD and the def2-SVP basis set.

UV–visible (UV-*Vis*) absorption. UV-*Vis* spectra were obtained by a Cary 5000 UV-*Vis* spectrophotometer. The diluted solution of CH45 was kept at a low concentration of 10^{-5} M.

Thermogravimetric (TGA) analysis. The TGA was carried out on a NETZSCH STA 409PC instrument under purified nitrogen gas flow. The heating rate is a 10 °C min^{-1}.

Cyclic voltammetry (CV). The CV experiments of CH45 were performed with a LK98B II Microcomputer-based Electrochemical Analyzer. All measurements were conducted at room temperature with a three-electrode configuration, including a glassy carbon electrode as the working electrode, a saturated calomel electrode (SCE) as the reference electrode, and a Pt wire as the counter electrode. Tetrabutyl ammonium phosphorus hexafluoride (n-Bu_4NPF_6, 0.1 M) in acetonitrile was employed as the supporting electrolyte, and the scan rate was kept at 100 mV s^{-1}. Electrochemically reversible ferrocene was employed as internal reference. The HOMO and LUMO energy levels were calculated from the onset oxidation and the onset reduction potentials, respectively, by following the equation $E_{\mathrm{HOMO}} = -(4.80+E_{\mathrm{ox}}^{\mathrm{onset}})$ eV, $E_{\mathrm{LUMO}} = -(4.80+E_{\mathrm{re}}^{\mathrm{onset}})$ eV.

Single-crystal growth. Single crystals of CH45 were grown by the liquid diffusion method at room temperature. In detail, 5 mL of methanol was transferred to 0.2 mL of concentrated chloroform or CN solution of CH45 slowly, and the beautiful dark purple crystals were formed on the inner glassy tube after about 2-10 days. The X-ray diffraction signals of single crystal were collected on Rigaku XtalAB PRO MM007 DW. The crystal was kept at 193(2) K during data collection.

Atomic force microscopy (AFM). The AFM images were performed using in tapping mode on a Bruker Dimension Icon atomic force microscope.

Grazing incidence wide angle X-ray scattering (GIWAXS). The GIWAXS samples were deposited on Si substrates by the same preparation conditions with devices and were carried out at Xenocs/Xeuss 2.0 equipment.

Photoluminescence (PL). The PL measurements were conducted by using FLS1000 equipment. The corresponding emission spectra were obtained using the same setup used for recording electroluminescence spectra excited by a 760 nm wavelength provided by Xenon lamp. (Detector for NIR 5509 PMT, 600-1700nm).

Electroluminescence (EL). The OSCs used for the EL spectra measurements are the same with those of the J-V measurements, with the conversional device structure of

ITO/PEDOT:PSS (4083)/PM6:NFAs / PNDIT-F3N/Ag. The EL spectra are measured by using a source meter (Keithley 2400) to inject electric current (1 mA), and the emitted photons were measured using a fluorescence spectrometer (KYMERA- 328I-B2, Andor technology LTD) with two sets of diffraction gratings, coupled to a Si EMCCD camera (DU970P-BVF, Andor) for the wavelength range of 400-1000 nm, and an InGaAs camera (DU491A-1.7, Andor) for the wavelength range of 900-1700 nm was used to collect the photons emitted from the solar cell.

EQE_{EL}. For the EQE_{EL} measurements, a digital source meter (Keithley 2400) was employed to inject electric current into the solar cells, and the emitted photons were collected by a Si diode (Hamamatsu s1337-1010BQ) and indicated by a picoammeter (Keithley 6482).

Highly sensitive EQE (sEQE). sEQE measurements were conducted by using a measurement system containing a halogen lamp light source (LSH-75, Newport), a monochromator (CS260-RG-3-MC-A, Newport), a current amplifier, a chopper and a phase-locked amplifier (SR830, Newport). The overtone signals from the monochromator were blocked by a group of long pass filters (1100 nm, 900 nm, 600 nm).

Device fabrication and measurement. The conventional devices based on PM6: Acceptors were fabricated with an architecture of ITO/PEDOT:PSS (4083)/PM6: Acceptor s/PNDIT-F3N/Ag. In detail, the ITO glass was pre-cleaned in turn in an ultrasonic bath of detergent, deionized water, acetone and isopropanol. Then the surface of ITO was treated by UV light in an ultraviolet-ozone chamber (Jelight Company) for 15 min. A thin layer of poly(3,4-ethylene dioxythiophene):poly(styrene sulfonate) (PEDOT:PSS, Baytron PVP Al 4083) was prepared by spin-coating the PEDOT:PSS solution at 4300 rpm for 20 s on the ITO substrate. Note that the PEDOT:PSS solution was pre-filtered through a 0.45 mm poly(tetrafluoroethylene) (PTFE) filter. Subsequently, the PEDOT:PSS films were baked at 150 °C for 20 min in air and transferred to a glove box filled with argon. Then the PM6:CH45 (D/A 1:1.2) and

PM6:CH45 (D/A 1:1.2) with 0.6% 1-chloronaphthalene mixtures were fully dissolved in chloroform (CF) at a concentration of 6 mg/mL of PM6 respectively, and the resulting solutions were spin-casted at 2000 rpm for 30 s onto the PEDOT:PSS layer. And then the films (PM6:CH45 (D/A 1:1.2) with 0.6% 1-chloronaphthalene) were treated with or without the thermal annealing (TA) at 90˚C for 5 min, or solvent vapor annealing (SVA) in DCM for 5 min. The best active layer thickness is about 110 nm. After that, about 15 nm thickness of PNDIT-F3N (dissolved in methanol with the concentration of 1 mg/mL) layer was spin-coated on the top of the active layer. Finally, a layer of Ag with thickness of 150 nm was deposited under 2×10^{-6} Pa. The active area of the device was 4 mm^2. The current density-voltage (*J*-*V*) curves of photovoltaic devices were recorded by a Keithley 2400 source-measure unit. The photocurrent was measured under the simulated illumination of 100 mW cm^{-2} with AM1.5 G using a Enli SS-F5-3A solar simulator, which was calibrated by a standard Si solar cell (made by Enli Technology Co., Ltd., Taiwan, and calibrated report can be traced to NREL). The thickness of the active layers was measured by a Veeco Dektak 150 profilometer. The EQE spectra were measured by using a QE-R Solar Cell. Response Measurement System (Enli Technology Co., Ltd., Taiwan).

Space-charge-limited current (SCLC) measurement. The SCLC method was used to measure the hole and electron mobilities, by using a diode configuration of ITO /PEDOT:PSS/active layer/MoO_3/Al for hole-only device and ITO/ZnO/active layer/ PNDIT-F3N/Al for electron-only device. In our case, we applied forward scans for all the SCLC measurements, and hence the ITO and Al electrodes should be the anode and cathode, respectively. The dark current density curves were recorded with a bias voltage in the range of 0-8 V. The mobilities were estimated by taking current-voltage curves and fitting the results based on the equation listed below:

$$J = \frac{9\varepsilon_0\varepsilon_\gamma\mu V^2}{8L^3}$$

where J is the current density, ε_0 is the vacuum permittivity, ε_r is the relative dielectric constant, μ is the mobility, and L is the film thickness. V ($=V_{\mathrm{app}} - V_{\mathrm{bi}}$) is the internal voltage in the device, where V_{app} is the applied voltage to the device and V_{bi} is the built-in voltage due to the relative work function difference of the two electrodes.

2. Synthesis of CH45.

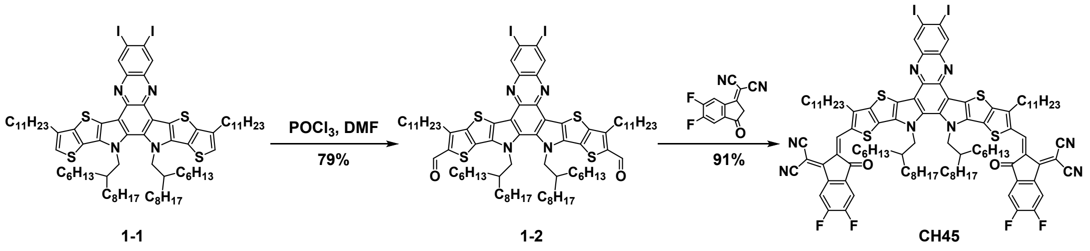

Scheme S1. The overall synthetic route to CH45.

Synthesis of compound 1-2. Under the protection of argon, phosphorus oxychloride (0.2 mL) was added to a solution of compound 1-1 (321 mg, 0.215 mmol, 1.0 eq.) and *N*, *N*-Dimethylformamide (DMF, 0.25 mL) in 1, 2-dichloroethane ($ClCH_2CH_2Cl$, 35 mL). The resulting mixture was stirred and heated to reflux for 12 h, then was cooled to 0°C. The resulting mixture was slowly added a saturated solution sodium acetate (45 mL), then was stirred at room temperature for 1 h. The resulting mixture was extracted with dichloromethane and the organic layer was dried over anhydrous Na_2SO_4 for 30 min. After removal of solvent, the crude product was then purified by column chromatography on silica gel to afford compound 1-2 as a red solid (263 mg, 79%).

Data for compound 1-2: ^{1}H NMR (400 MHz, $CDCl_3$) δ 10.15 (s, 1H), 8.82 (s, 1H), 4.70 (d, J = 7.3 Hz, 2H), 3.17 (s, 2H), 2.19 (s, 1H), 2.02-1.76 (m, 2H), 1.54-1.44 (m, 2H), 1.41-1.21 (m, 16H), 1.12-0.91 (m, 20H), 0.90-0.81 (m, 5H), 0.76 (t, J = 7.2 Hz, 3H), 0.67 (t, J = 6.5 Hz, 3H). ^{13}C NMR (101 MHz, $CDCl_3$) δ 181.85, 146.82, 144.51, 140.70, 138.77, 138.31, 136.85, 136.75, 132.48, 129.42, 128.03, 117.46, 107.24, 55.59, 39.18, 31.92, 31.76, 31.63, 30.57, 29.83, 29.70, 29.64, 29.56, 29.47, 29.39, 29.35, 29.17, 28.19, 25.73, 25.67, 22.70, 22.56, 22.49, 14.13, 14.05, 13.95. HRMS (m/z, MALDI): Calc. for $[C_{80}H_{116}I_2N_4O_2S_4]H^+$. 1547.6143, found: 1547.6066.

Synthesis of compound CH45. Under the protection of argon, dry pyridine (0.3 mL) was added to a solution of compound 1-2 (198 mg, 0.128 mmol, 1.0 eq.) and 2-

(5,6-difluoro-3-oxo-2,3-dihydro-1H-inden-1-ylidene) malononitrile (88 mg, 0.384 mmol 3.0 eq.) in chloroform ($CHCl_3$, 30 mL). The resulting mixture was stirred and heated to reflux for 12 h. After being cooled to room temperature, the solvent was removed under vacuum. The crude product was then purified by column chromatography on silica gel to afford CH45 as a black and blue solid (229 mg, 91%).

Data for CH45: ^{1}H NMR (400 MHz, $CDCl_3$) δ 9.07 (s, 1H), 8.76-8.50 (m, 1H), 8.43 (s, 1H), 7.75 (t, J = 7.4 Hz, 1H), 4.91 (d, J = 6.5 Hz, 2H), 3.15 (s, 2H), 2.40 (s, 1H), 1.83 (s, 2H), 1.55-0.99 (m, 40H), 0.86 (t, J = 6.7 Hz, 3H), 0.77-0.65 (m, 6H). ^{13}C NMR (101 MHz, $CDCl_3$) δ 186.17, 158.52, 155.80, 155.66, 153.81, 153.21, 153.04, 146.66, 140.39, 138.37, 137.66, 136.51, 135.96, 134.98, 134.51, 133.40, 133.22, 131.37, 119.65, 118.63, 115.01, 114.84, 114.50, 112.57, 108.17, 68.31, 55.96, 39.76, 31.94, 31.87, 31.81, 31.44, 30.85, 30.16, 30.03, 29.85, 29.75, 29.69, 29.66, 29.61, 29.39, 29.28, 26.06, 22.70, 22.59, 22.57, 14.13, 14.06, 14.03. HRMS (*m*/*z*, MALDI): Calc. for $C_{104}H_{120}F_4I_2N_8O_2S_4$. 1971.6476, found: 1971.6474.

3. Figures and Tables.

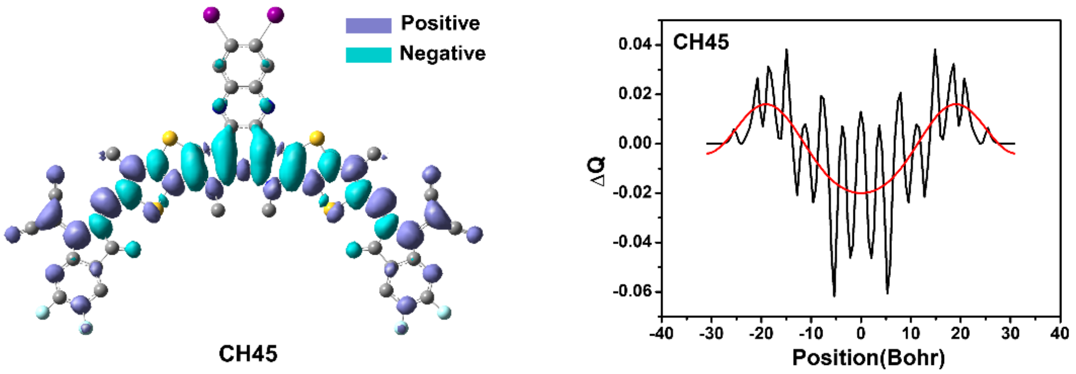

Figure S1. Theoretical density distribution ΔQ ($\Delta Q = \Psi^{2}{}_{\mathrm{LUMO}} - \Psi^{2}{}_{\mathrm{HOMO}}$) along the longest axis of CH45. Black curves are the integral lines of the charge density difference (ΔQ) along the longest axis of CH45. Red curves are the simulated results with low frequencies wave functions by fast fourier transform filters.

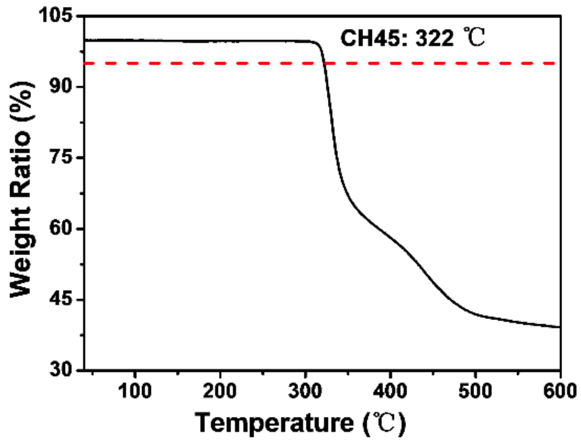

Figure S2. Thermogravimetric analysis (TGA) curve of CH45. The heating rate is a heating rate of 10 ºC/min under nitrogen atmosphere.

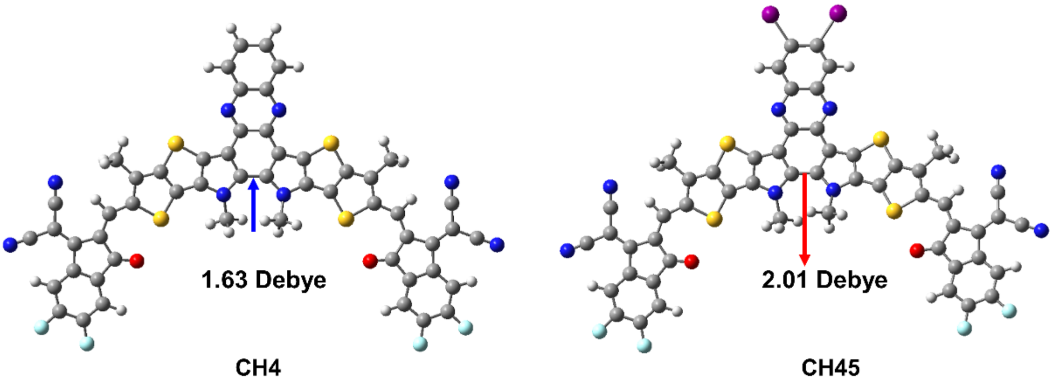

Figure S3. The dipole moment of CH4 and CH45 by DFT calculation.

Table S1. Ionization potential (IP), electron affinity (EA), transport gap (E_g^t), optical gap (E_g^O), and exciton binding energy (E_b) of CH4 and CH45 in gas phase.

Comp	IP/eV	EA/eV	E_g^t/eV	E_g^O/eV	E_b/eV
CH4	6.243	2.791	3.452	1.792	1.660
CH45	6.328	2.877	3.451	1.842	1.609

[a] $E_g^t = IP - EA$; [b] $E_b = E_g^t - E_g^O$.

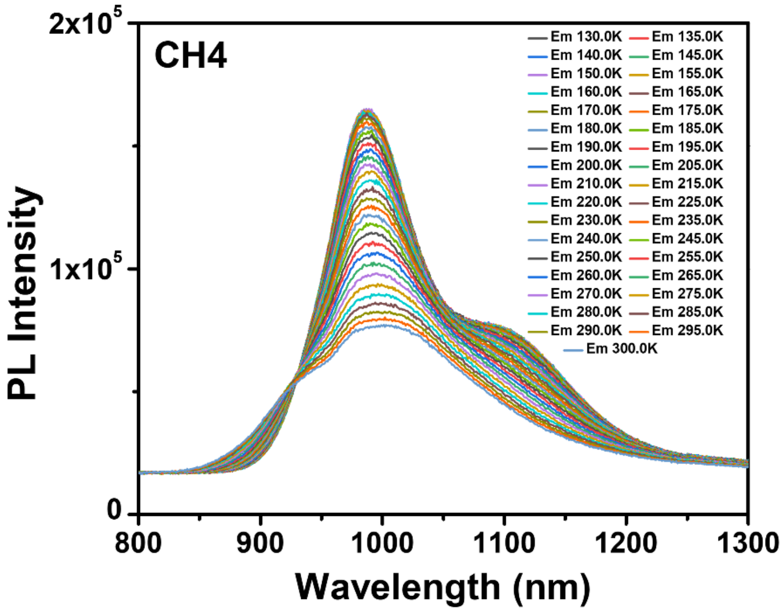

Figure S4. Temperature-dependent PL spectra of CH4 in thin films.

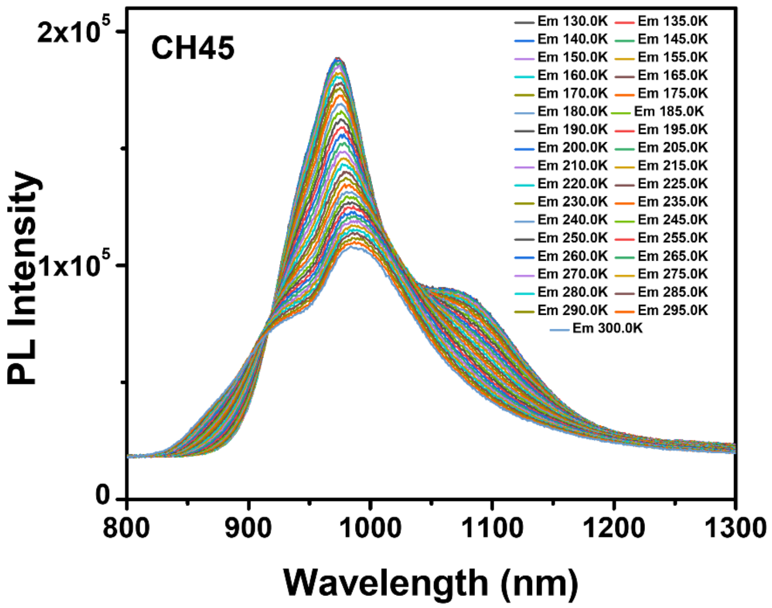

Figure S5. Temperature-dependent PL spectra of CH45 in thin films.

Table S2. The optical and electrochemical data of acceptors in this work.

Comp	$\lambda_{max}^{sol[a]}$ (nm)	$\lambda_{max}^{film[b]}$ (nm)	λ_{edg}^{film} (nm)	$\Delta\lambda^{[c]}$ (nm)	$E_g^{onset[d]}$ (eV)	HOMO[e] (eV)	LUMO[e] (eV)	$\varepsilon^{[f]}$ (10^5 M^{-1} cm^{-1})
CH4	752	818	910	66	1.36	–5.64	–3.84	1.41
CH45	742	816	903	74	1.37	–5.66	–3.85	1.58

[a] λ_{max}^{sol} was obtained from UV-*Vis* absorption spectra of CH4 and CH45 in chloroform solutions. [b] Δλ represents the redshift (Δλ) from solution to film. [c] λ_{max}^{film} was obtained from UV-*Vis* absorption spectra of `CH4 and CH45 in films. [d] Optical band gap (E_g^{onset}) was calculated by $1240/\lambda_{edge}^{film}$. [e] The highest occupied molecular orbital (HOMO) and lowest unoccupied molecular orbital (LUMO) energy levels were calculated from the onset oxidation potential and the onset reduction potential using the equation $E_{HOMO} = - (4.80+E_{ox}^{onset})$ eV, $E_{LUMO} = - (4.80+E_{re}^{onset})$ eV. [f] ε is molar extinction coefficient obtained from UV-Vis absorption spectra of CH4 and CH45 in chloroform solution.

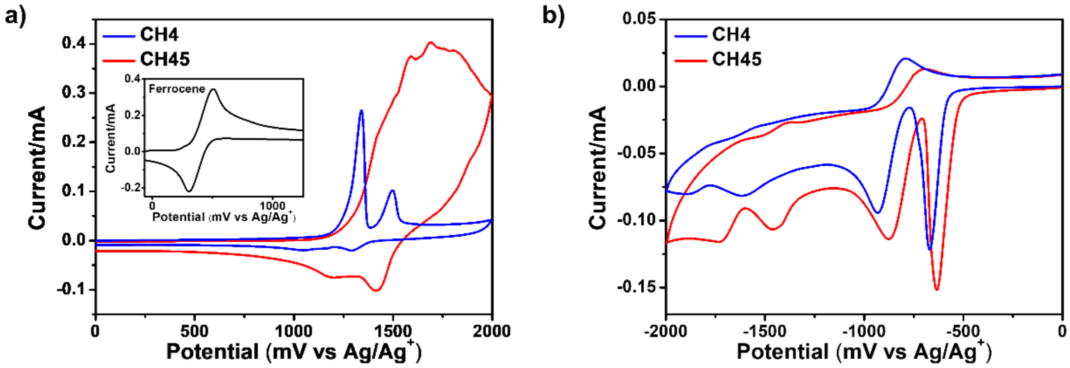

Figure S6. Cyclic voltammograms of the reference (ferrocene), CH4 and CH45 films, respectively. a) Oxidation and reduction cycle of ferrocene; oxidation cycle of CH4 and CH45 films, respectively; b) reduction cycle of CH4 and CH45 films, respectively.

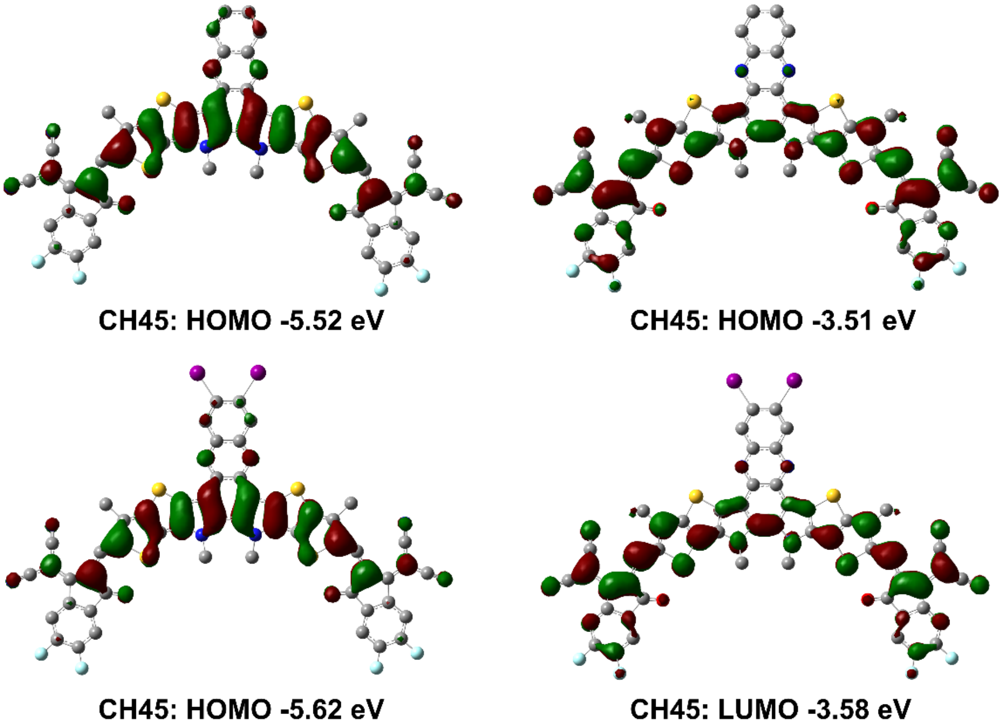

CH45: HOMO -5.52 eV

CH45: HOMO -3.51 eV

CH45: HOMO -5.62 eV

CH45: LUMO -3.58 eV

Figure S7. Theoretical density distribution for the frontier molecular orbits of CH4 and CH6.

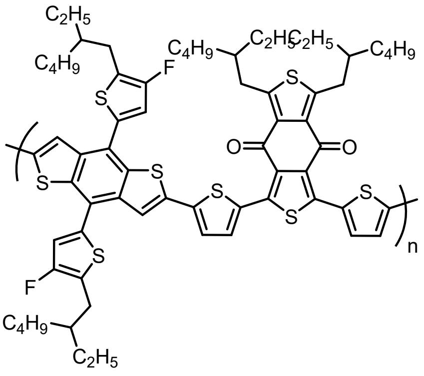

PM6

Figure S8. The structure of polymer donor PM6.

Table S3. Detailed photovoltaic parameters of the PM6:CH45 based devices by optimal conditions under illumination of AM 1.5 G, 100 mW/cm^2. [a]

Active layer	V_{oc} [V]	J_{sc} [mA cm^{-2}]	FF [%]	PCE [%]
PM6:CH45	0.910	25.56	73.3	17.05
	0.908	25.74	72.8	17.02
	0.905	25.74	72.9	16.99
	0.906	25.42	72.9	16.80
	0.908	25.55	72.7	16.85
	0.906	25.72	72.6	16.91
	0.910	25.54	71.8	16.69
	0.912	25.32	72.6	16.76
	0.910	25.45	72.4	16.77
	0.913	25.26	72.6	16.75
	0.906	25.42	72.9	16.80
	0.904	25.28	73.0	16.68
	0.912	25.34	73.7	17.03
	0.907	25.32	73.0	16.76
	0.910	25.39	73.0	16.86
Average[b]	0.908	25.47	72.8	16.85

[a] The device architecture is ITO/PEDOT:PSS/active layer/PNDIT-F3N/Ag; D = 6mg/mL in chloroform; the resulting solutions were spin-casted at 2000 rpm for 30s onto the PEDOT:PSS layer.

[b] The average values are obtained from 15 devices.

Table S4. Detailed photovoltaic parameters of the PM6:CH45 (CN) based devices by optimal conditions under illumination of AM 1.5 G, 100 mW/cm^2. [a]

Active layer	V_{oc} [V]	J_{sc} [mA cm^{-2}]	FF [%]	PCE [%]
PM6:CH45 (CN)	0.913	25.41	77.5	17.97

	0.908	25.83	77.1	18.09
	0.907	25.85	76.9	18.03
	0.910	25.57	78.0	18.14
	0.909	25.57	77.4	17.98
	0.909	25.38	77.7	17.92
	0.909	25.43	77.6	17.95
	0.914	25.49	77.2	17.97
	0.912	25.77	76.8	18.04
	0.913	25.20	78.0	17.95
	0.910	25.42	77.7	17.96
	0.908	25.19	78.3	17.91
	0.909	25.67	77.3	18.04
	0.911	25.38	77.7	17.97
	0.906	25.35	78.7	18.08
Average[b]	0.910	25.50	77.6	18.00

[a]The device architecture is ITO/PEDOT:PSS/active layer/PNDIT-F3N/Ag; D = 6mg/mL in chloroform with 0.5 vol% CN; the resulting solutions were spin-casted at 2000 rpm for 30s onto the. [b]The average values are obtained from 15 devices.

Table S5. Detailed photovoltaic parameters of the PM6:CH4 based devices by optimal conditions under illumination of AM 1.5 G, 100 mW/cm^2. [a]

Active layer	V_{oc} [V]	J_{sc} [mA cm^{-2}]	FF [%]	PCE [%]
PM6:CH4	0.901	24.16	66.0	14.37
	0.904	24.29	66.1	14.52
	0.904	24.06	67.9	14.77
	0.899	24.01	67.3	14.53
	0.908	24.67	66.4	14.87
	0.904	24.27	66.2	14.52
	0.899	24.15	66.7	14.47
	0.907	24.15	66.8	14.64
	0.900	24.27	66.8	14.58
	0.906	24.53	66.3	14.73
	0.902	24.34	65.9	14.46
	0.908	24.05	67.2	14.66
	0.909	24.64	66.3	14.86
	0.904	24.25	66.9	14.68
	0.900	24.12	67.1	14.56
Average[b]	0.904	24.26	66.7	14.61

[a]The device architecture is ITO/PEDOT:PSS/active layer/PNDIT-F3N/Ag; D = 6mg/mL in chloroform; the resulting solutions were spin-casted at 2000 rpm for 30s onto the PEDOT:PSS layer; TA (90 °C for 5 min). [b]The average values are obtained from 15 devices.

Table S6. Detailed photovoltaic parameters of the PM6:CH4 (CN) based devices by optimal conditions under illumination of AM 1.5 G, 100 mW/cm^2.[a]

Active layer	V_{oc} [V]	J_{sc} [mA cm^{-2}]	FF [%]	PCE [%]
PM6:CH4 (CN)	0.898	23.44	74.1	15.59
	0.891	23.17	74.4	15.36
	0.884	22.96	75.1	15.24
	0.898	23.73	74.7	15.90
	0.893	22.97	74.6	15.29
	0.887	22.81	74.7	15.11
	0.885	22.76	75.0	15.10
	0.896	23.67	75.0	15.90
	0.888	23.05	74.9	15.32
	0.886	23.13	74.9	15.34
	0.894	23.22	74.5	15.48
	0.89	22.99	74.8	15.30
	0.887	22.80	74.2	15.01
	0.885	22.85	74.5	15.06
	0.882	22.55	74.9	14.90
Average[b]	0.890	23.07	74.7	15.33

[a] The device architecture is ITO/PEDOT:PSS/active layer/PNDIT-F3N/Ag; D = 6mg/mL in chloroform with 0.5 vol% CN; the resulting solutions were spin-casted at 2000 rpm for 30s onto the PEDOT:PSS layer). [b] The average values are obtained from 15 devices.

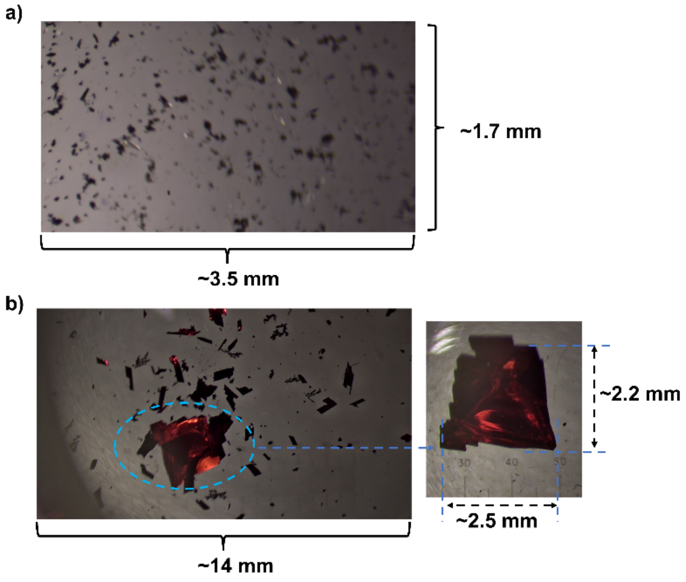

Figure S9. Single-crystal photos of CH45 a) in chloroform (CF) and b) in 1-chloronaphthalene (CN), respectively (From microscope).

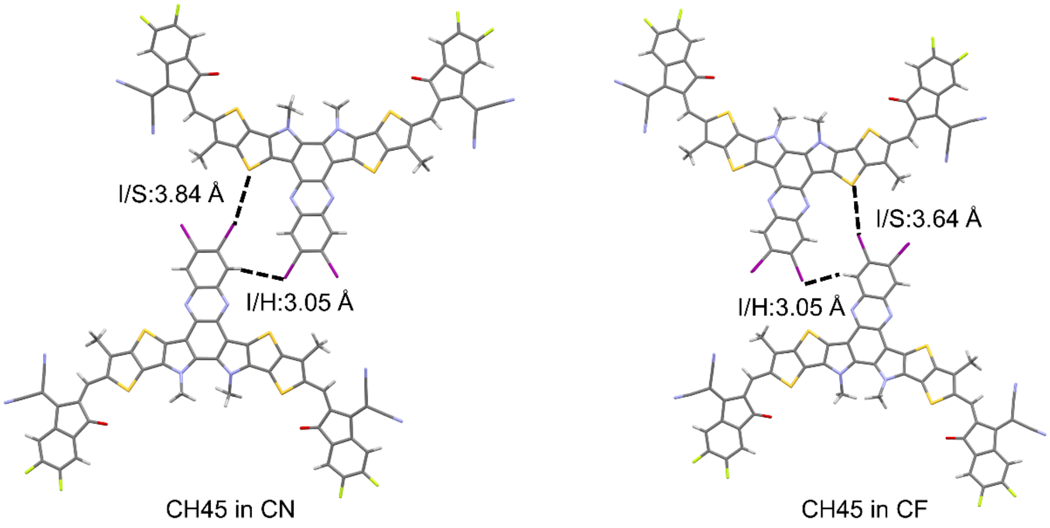

Figure S10. The molecular pair was formed through weak I-S/I-H secondary intermolecular interactions in CH45 single crystal.

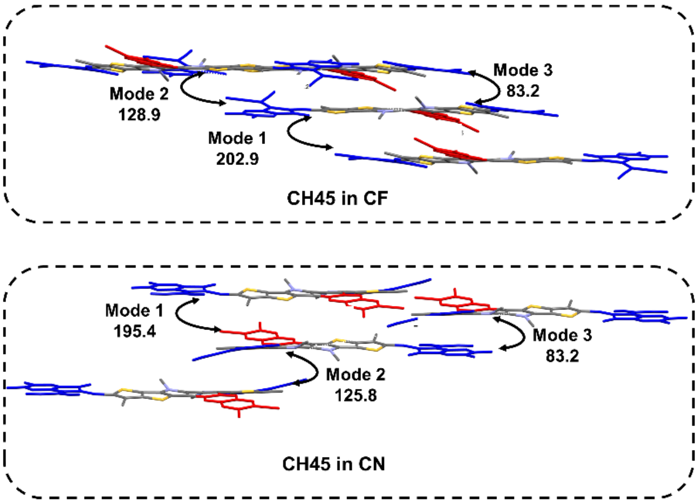

Figure S11. Main UNI inter-molecular potentials (> |80| kJ/mol) and the corresponding defined modes of CH45 with respect to nearest neighbors by Mercury software (kJ/mol). The inter-molecular potentials were obtained by method described in section: computational methods.

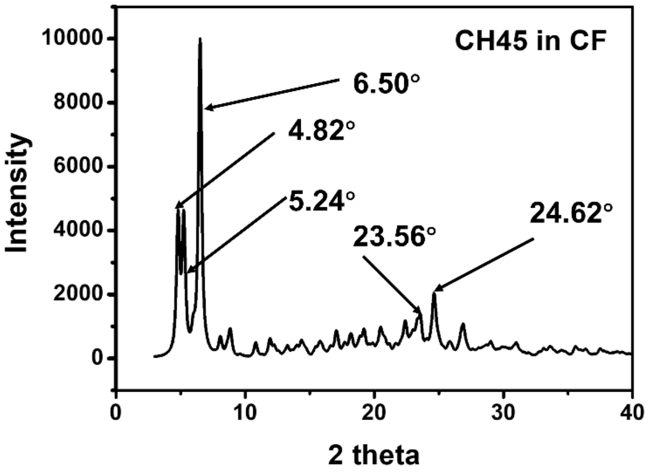

Figure S12. CH45 X-ray diffraction pattern generated with Mercury CSD software using CH45 single crystal diffraction data (in CF). According to the Bragg equation $2d\sin\theta = \lambda$ and $d = 2\pi/q$, there are strong peaks at 2θ = 4.82, 5.24, 6.50, 23.56 and 24.62° observed in X-ray diffraction pattern generated from single crystal structure data of CH45, corresponding to the packing distances of 18.32, 16.85, 13.59, 3.77 and 3.61 Å, respectively.

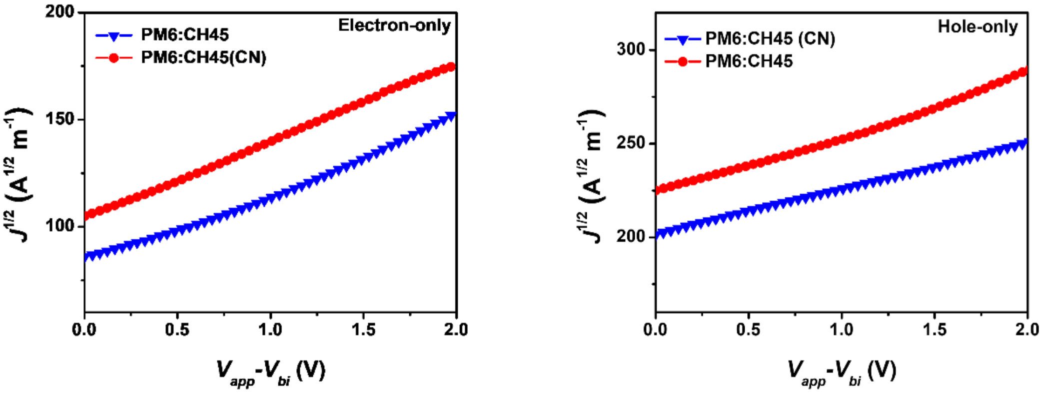

Figure S13. SCLC characteristics of electron-only and hole-only of PM6:CH45, and PM6:CH45(CN) blend films. The electron/hole mobilities (μ_e/μ_h) of PM6:CH45 based blend films with and without CN were $5.9\times10^{-4}/4.4\times10^{-4}$ and $5.0\times10^{-4}/2.6\times10^{-4}$ V^{-1} s^{-1}, with corresponding to μ_e/μ_h ratios of 1.3 and 1.9, respectively.

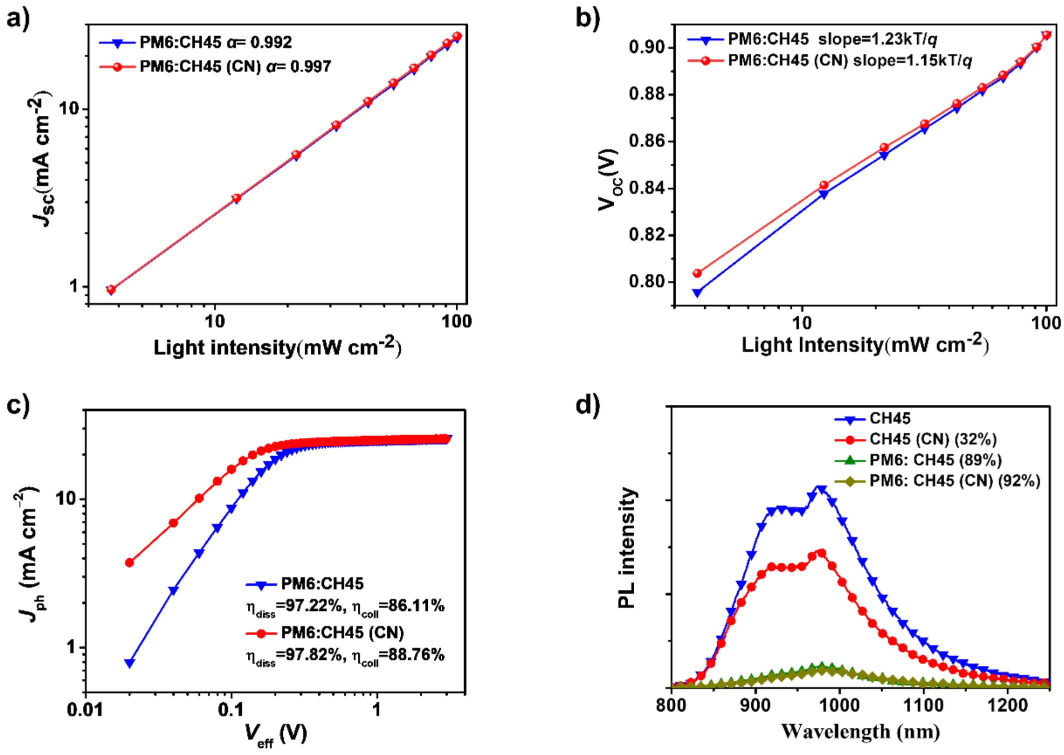

Figure S14. a) Dependences of current density (J_{sc}) on P_{light} of optimized OSCs. b) Dependences of V_{oc} on P_{light} of optimized OSCs.c) Plots of J_{ph} versus V_{eff}. d) Photoluminescence spectra of neat and blend films.

Table S7. Total energy loss values and different contributions in solar cells based on the SQ limit theory.

Active layer	V_{OC} (V)	E_g[a] (eV)	$V_{OC,}$ SQ[b] (V)	$V_{OC,}$ rad[b] (V)	ΔE_1[c] (eV)	ΔE_2[d] (eV)	ΔE_3[e] (eV)	E_{loss}[f] (eV)
PM6:CH45	0.912	1.431	1.167	1.118	0.264	0.049	0.206	0.519
PM6:CH45(CN)	0.910	1.436	1.172	1.122	0.264	0.050	0.212	0.526

[a] E_g is estimated on the basis of the derivatives of the EQE spectra (dEQE/dE, black curves) (Figure S16). [b] V_{OC}^{SQ} is the upper limit for the V_{OC} of the solar cell derived in the Shockley-Quessier theory. V_{OC}^{rad} is the radiative recombination limit for the V_{OC} of the solar cell, which can be

determined by the equation: $$V_{OC}^{SQ}=\frac{kT}{q}\ln\left(\frac{J_{SC}^{SQ}}{J_{0}^{SQ}}+1\right)\cong\frac{kT}{q}\ln\left(\frac{q\cdot\int_{E_g}^{+\infty}\emptyset_{AM1.5G}(E)dE}{q\cdot\int_{E_g}^{+\infty}\emptyset_{BB}(E)dE}\right)$$ [c]

$\Delta E_1=E_g-qV_{OC}^{SQ}$; [d] $\Delta E_2=qV_{OC}^{SQ}-qV_{OC}^{rad}$; $J_{0,\mathrm{rad}}=q\int \mathrm{EQE}(E)\emptyset_{\mathrm{BB}}(E)\mathrm{d}E$; $V_{\mathrm{OC}}^{\mathrm{rad}}=\frac{k_{\mathrm{B}}T}{q}\mathrm{In}(\frac{J_{\mathrm{SC}}}{J_{0,\mathrm{rad}}}+1)$; [e]

$\Delta E_3=qV_{\mathrm{OC}}^{\mathrm{rad}}-qV_{\mathrm{OC}}$; [f] $E_{\mathrm{loss}}=\Delta E_1+\Delta E_2+\Delta E_3$.

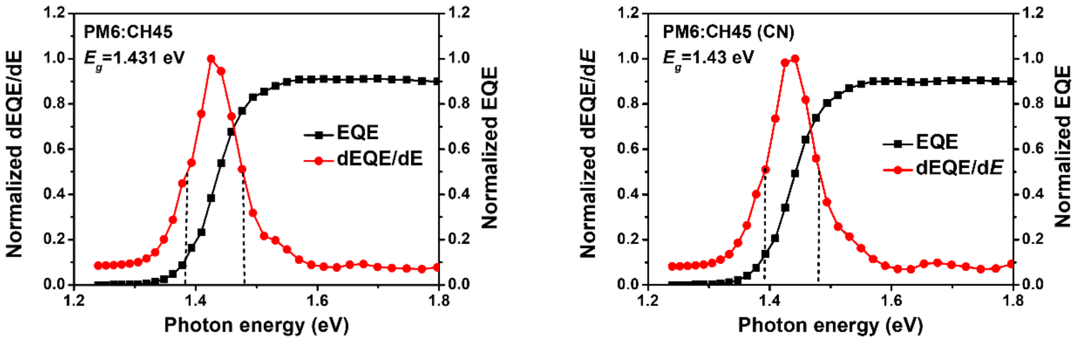

Figure S15. Optical bandgap determination of PM6:CH45 and PM6:CH45 (CN) on the basis of the derivatives of the EQE spectra (dEQE/dE, red curves). The region between dashed lines is the part where the gap distribution probability is greater than half of the maximum, which is used for the bandgap calculation.

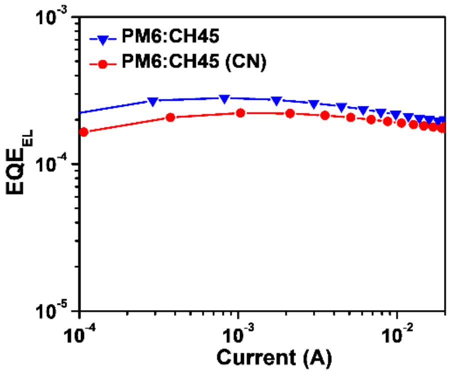

Figure S16. EQE_{EL} spectra of PM6:CH45 and PM6:CH45 (CN) based OSCs, EQE_{EL} values for PM6:CH45 and PM6:CH45 (CN) based devices are 2.80×10^{-4} and 2.22×10^{-4}, respectively.

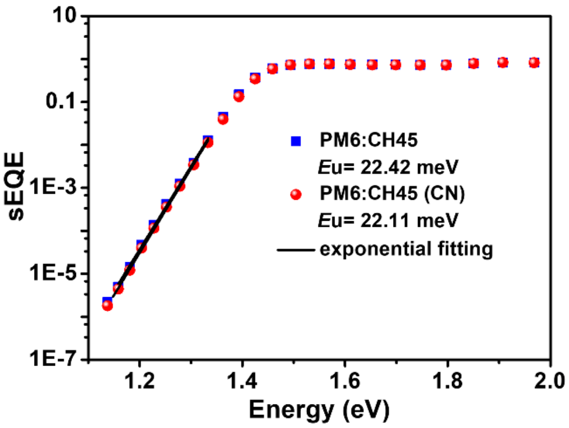

Figure S17. Analysis of energetic disorder of optimized PM6:CH45 based OSCs with and without CN at the absorption onset of sensitive external quantum efficiency spectra (sEQE).

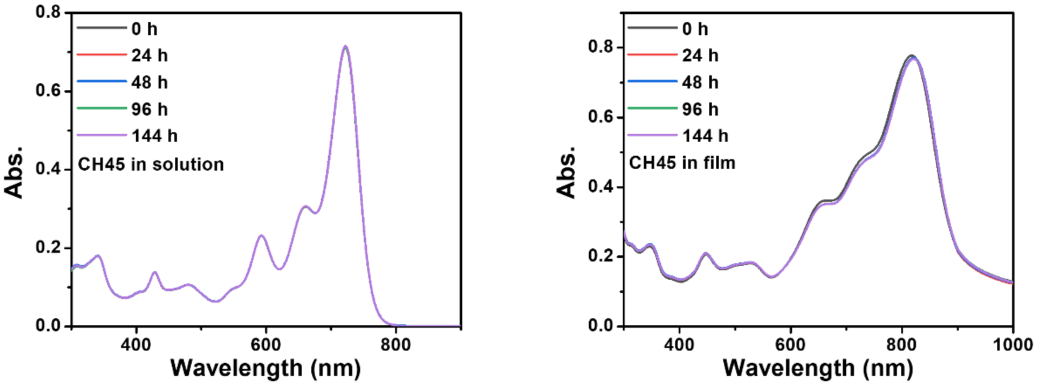

Figure S18. Photo stability. UV-vis absorption spectra plotted vs. aging time under continuous illumination of CH45 in dilute toluene solutions and in films.

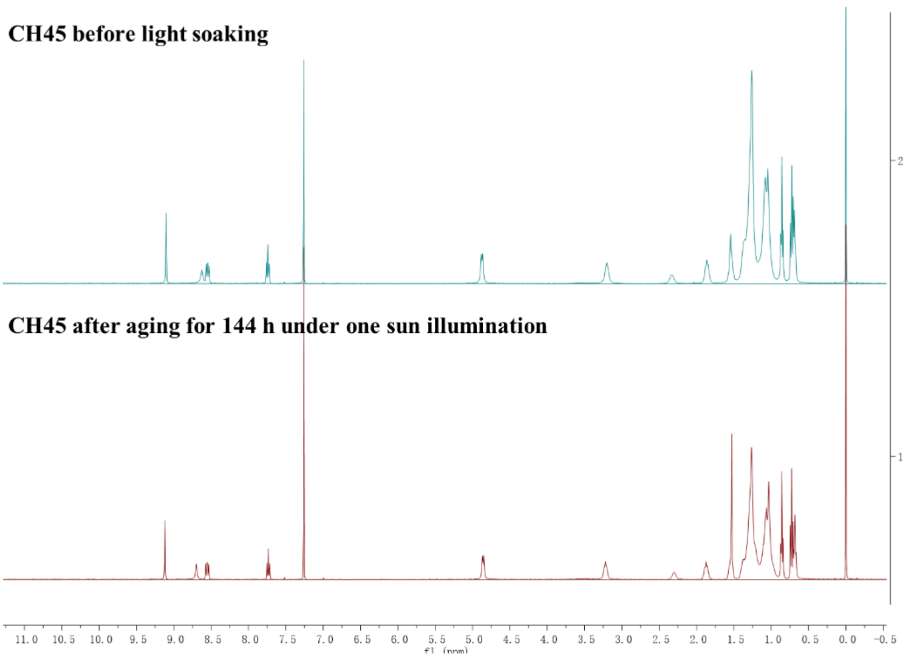

Figure S19. Photo stability. ^{1}H NMR spectra of CH45 fresh and aged samples in $CDCl_3$.

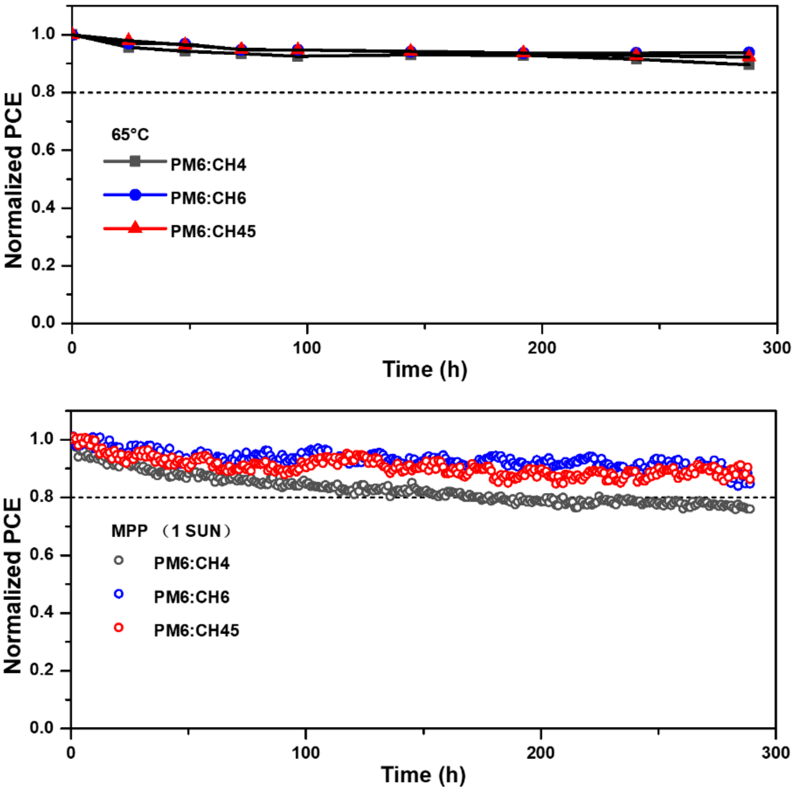

Figure S20. Thermal stability and photo-stability of CH45 blends-based optimal devices.

3.4 NMR spectra and MS.

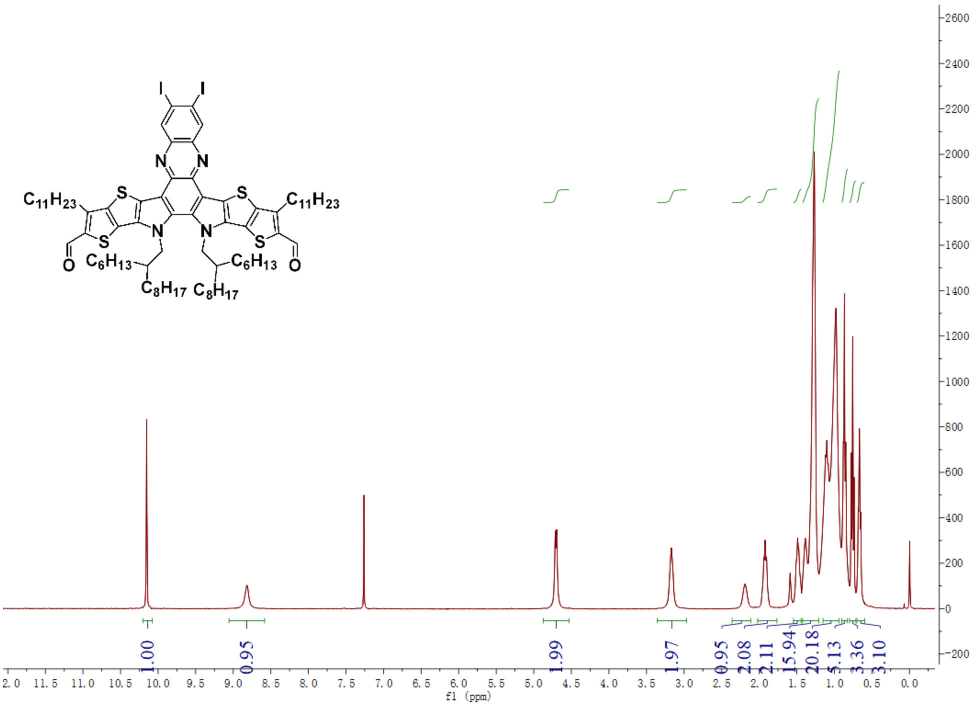

Figure S21. ^{1}H NMR spectrum of compound 1-2 at 300K in CDCl$_3$.

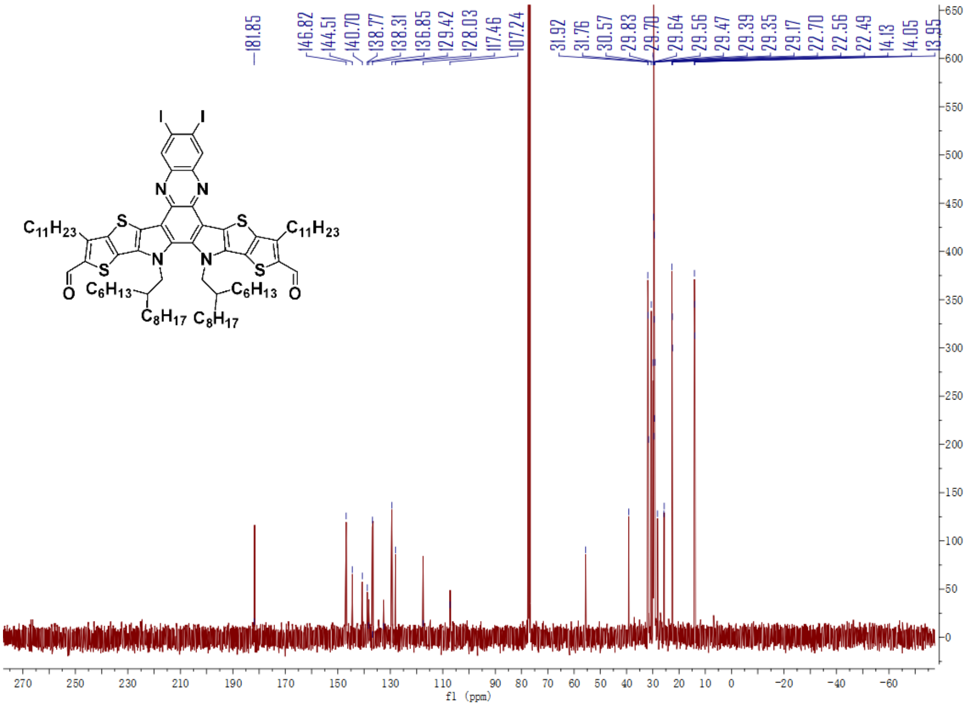

Figure S22. ^{13}C NMR spectrum of compound 1-2 at 300K in CDCl$_3$.

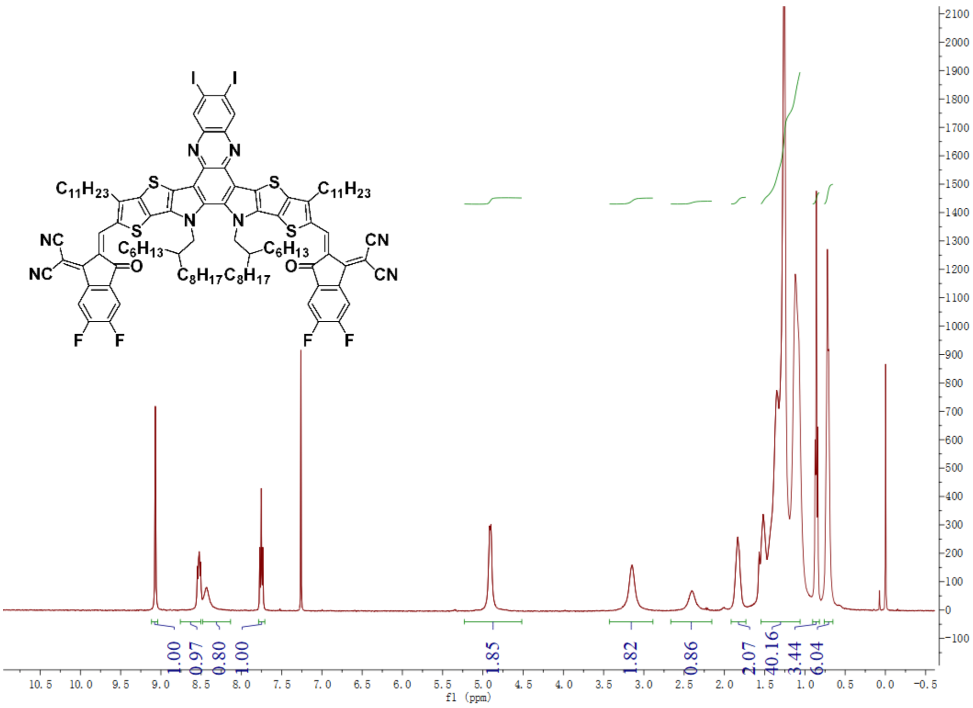

Figure S23. ^{1}H NMR spectrum of CH45 at 300K in CDCl$_3$.

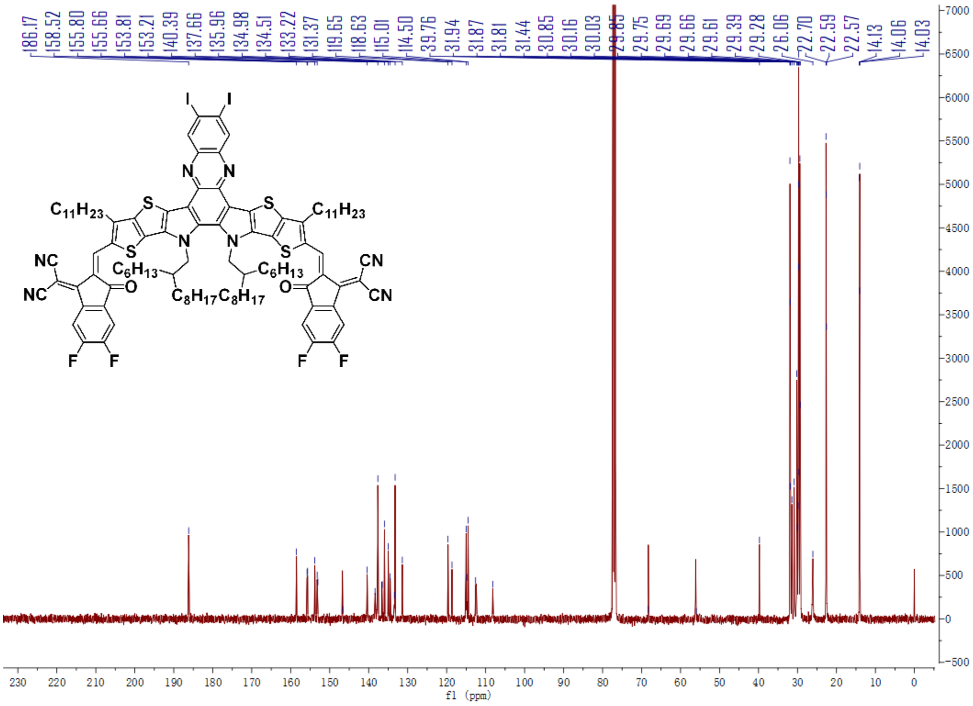

Figure S24. ^{13}C NMR spectrum of CH45 at 300K in CDCl$_3$.

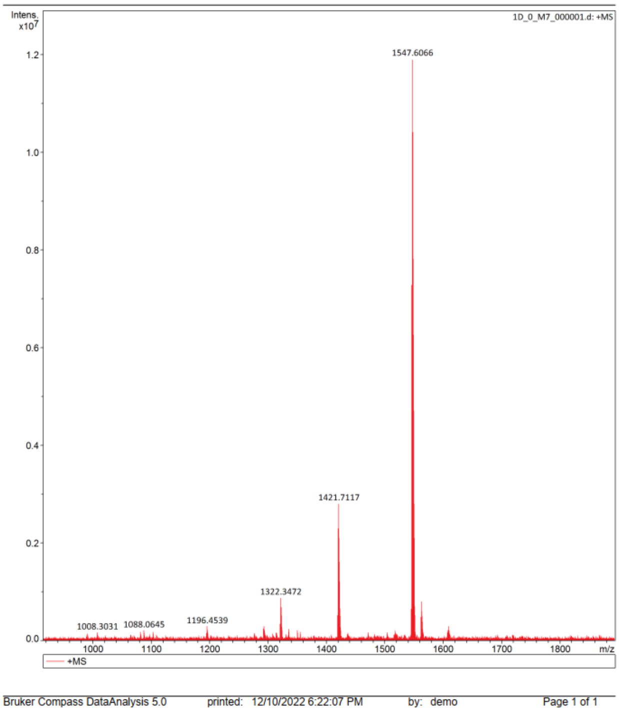

Figure 25. HRMS of compound 1-2.

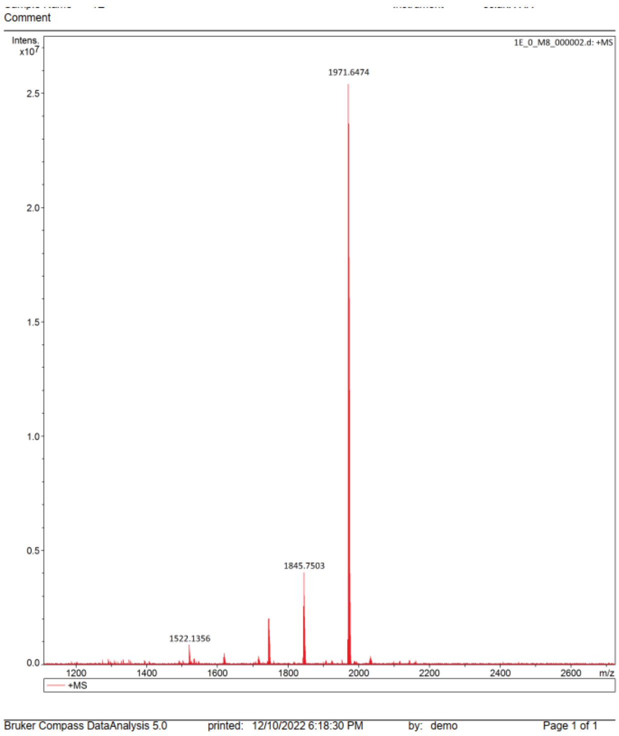

Figure 26. HRMS of CH45.

4. References.

[1] H. Chen, Y. Zou, H. Liang, T. He, X. Xu, Y. Zhang, Z. Ma, J. Wang, M. Zhang, Q. Li, C. Li, G. Long, X. Wan, Z. Yao, Y. Chen, *Sci. China Chem.* **2022**, *65*, 1362-1373.

[2] A. D. Becke, *J Chem Phys* **1993**, *98*, 5648-5652.

[3] P. C. Hariharan, J. A. Pople, *Mol. Phys.* **1974**, *27*, 209-214.

[4] P. J. Hay, W. R. Wadt, *J Chem Phys* **1985**, *82*, 299-310.

[5] MJ. Frisch, et al. Gaussian 16, Gaussian, Inc.: Wallingford, CT, 2016.

[6] M. P. Hughes, K. D. Rosenthal, N. A. Ran, M. Seifrid, G. C. Bazan, T.-Q. Nguyen, *Adv. Funct. Mater.* **2018**, *28*, 1801542.

[7] a) J. Ji, L. Zhu, X. Xiong, F. Liu, Z. Liang, *Adv. Sci.* **2022**, *9*, 2200864; b) L. Zhu, J. Zhang, Y. Guo, C. Yang, Y. Yi, Z. Wei, *Angew. Chem. Int. Ed.* **2021**, *60*, 15348-15353.

[8] Y. Li, X. Huang, H. K. M. Sheriff, S. R. Forrest, *Nat. Rev. Mater.* **2023**, *8*, 186-201.